Journal of Materials Chemistry A

PAPER

View Article Online
View Journal | View Issue

Cite this: J. Mater. Chem. A, 2015, 3, 15962

Flexible and porous catalyst electrodes constructed by Co nanoparticles@nitrogen-doped graphene films for highly efficient hydrogen evolution†

Dongman Hou,[a] Weijia Zhou,*[b] Kai Zhou,[b] Yucheng Zhou,[b] Jing Zhong,[a] Linjing Yang,[b] Jia Lu,[b] Guoqiang Li*[a] and Shaowei Chen[bc]

Received 29th May 2015
Accepted 25th June 2015

DOI: 10.1039/c5ta03905c

www.rsc.org/MaterialsA

The development of electrodes composed of non-noble-metal catalysts with both excellent activity and high stability for the hydrogen evolution reaction (HER) is essential for hydrogen production. In this work, a flexible and robust film electrode based on cobalt nanoparticles embedded into the interlamination of N-doped graphene film (Co@NGF) is fabricated by simple vacuum filtration combined with subsequently controlled calcination. This flexible three-dimensional (3D) nano-architecture film directly used as the electrode shows a low onset potential of only −14 mV (*vs.* RHE) with a small Tafel slope of 93.9 mV per dec for the HER in 0.5 M H_2SO_4. Stability tests through long term potential cycles and extended electrolysis confirm the perfect durability of Co@NGFs in acid media. The remarkable HER catalytic activity is derived from the electron penetration effect of cobalt nanoparticles as the core protected by N-doped graphene as the shell. It is worth noting that the Co@NGF electrodes, for the first time, used as both the anode and cathode in a two-electrode system open up new possibilities for exploring overall water splitting catalysts in an acid electrolyte. This development offers an attractive HER film electrode for large-scale water splitting technology.

Introduction

With the growing demand for energy and environmental protection on the global scale, development of technologies for clean and sustainable energy has been attracting increasingly intense attention. Hydrogen is considered as one of the most ideal energy carriers that can be an alternative to fossil fuels in the future because of its numerous advantages, such as high calorific value and environmentally friendly use.[1] Hydrogen generation through electrolysis of water offers an attractive avenue to store energy from renewable sources such as the sun.[2,3] Many solar water-splitting devices are designed to function in an acidic electrolyte, in which the state-of-the-art hydrogen-producing catalysts are based on noble metals like Pt. Although Pt-group noble metals are the most active electrocatalysts for the HER, their high costs severely limit their broad utilization in energy systems. Two-dimensional MoS_2 with exposed edges have been demonstrated to be a very promising electrocatalyst as an alternative to Pt catalysts for the HER in recent years.[4–12] However, there are some limits for MoS_2, such as, larger overpotentials, not cheap enough and no reported green synthesis process. Therefore, exploring the low cost, high catalytic stability and high electrocatalytic activities of HER catalysts still remains a major challenge. It is noteworthy that Co-based HER catalysts have been under intensive research recently.[13–19] Among those, carbon coated transition-metal nanoparticles have been widely investigated as catalysts for application in the HER because they are in line with the above requirements.[18,20–22] Zou *et al.*[18] reported the synthesis of cobalt embedded nitrogen-rich carbon nanotubes (CNTs), which were shown to be highly efficient electrocatalysts for the HER in a wide range of pH, with a small onset potential of −50 mV and a low Tafel slope (69 mV per dec) in 0.5 M H_2SO_4. Bao *et al.*[23] reported a hierarchical architecture that consists of ultrathin graphene shells (only 1–3 layers) that encapsulate a uniform CoNi nanoalloy to enhance its HER performance in acidic media. Density functional theory (DFT) calculations indicated that the ultrathin graphene shells strongly promote electron penetration from the CoNi nanoalloy to the graphene surface. In these pioneering studies, non-precious transition metals (*e.g.*, Co, Ni, *etc.*) were protected by carbon materials which protect the metals from acid erosion, at the same time, the density of carbon electronic states may be modulated by

[a]State Key Laboratory of Luminescent Materials and Devices, South China University of Technology, 381 Wushan Road, Guangzhou 510641, China. E-mail: msgli@scut.edu.cn

[b]New Energy Research Institute, School of Environment and Energy, South China University of Technology, Guangzhou Higher Education Mega Center, Guangzhou, Guangdong 510006, China. E-mail: eszhouwj@scut.edu.cn

[c]Department of Chemistry and Biochemistry, University of California, 1156 High Street, Santa Cruz, California 95064, USA

† Electronic supplementary information (ESI) available. See DOI: 10.1039/c5ta03905c

transition metal elements such that carbon may also serve as an active site for the HER.[24]

Binder-free films and three-dimensional (3D) electrode structures can effectively lead to enhanced HER catalytic activity.[20,25–28] For example, Li *et al.*[29] reported that MoS_x grown on graphene-protected 3D Ni foams possesses high HER activity and the hydrogen evolution rate reaches 302 mL g^{-1} cm^{-2} h^{-1} at an overpotential of 200 mV due to the increased catalyst loading and more catalytic sites. Qiao *et al.*[28] fabricated a 3D hybrid film by decorating the N-doped graphene hydrogel with molecular clusters (MoS_x), which shows a remarkable and stable catalytic activity toward the HER (−140.6 mV at 10 mA cm^{-2}) with a Tafel slope of 105 mV per dec.

Herein, we synthesized a free-standing flexible film constituted of cobalt nanoparticles wrapped by a N-doped graphene film (Co@NGF). The obtained flexible and robust Co@NGF is then directly evaluated as a HER electrode with high activity, favorable kinetics and strong durability toward the HER. Benefiting from the synergetic effect among the core–shell structure, N-doped treatment, cobalt nanoparticles and porous structure, the Co@NGF exhibits a remarkable electrocatalytic activity for the HER, with the onset potential at only −14 mV (*vs.* RHE), a low Tafel slope value of 93.9 mV per dec and excellent catalytic stability (seldom performance degradation after 50 000 s or 1000 cycles). In addition, the Co@NGFs used as both the anode and cathode in the two-electrode system exhibit high activity toward both the oxygen and hydrogen evolution reactions in acid electrolytes. The reported fabrication method of the 3D flexible electrode with high HER activity is easily scalable and with low production cost.

Experimental

Materials

All reagents were of analytical grade and used without further purification. Cobalt acetate ($C_4H_6O_4Co$), dicyandiamide (DCDA, $C_2H_4N_4$), graphite powders, sulfuric acid (H_2SO_4), sodium nitrate ($NaNO_3$), potassium permanganate ($KMnO_4$), potassium hydroxide (KOH) and 20 wt% Pt/C were purchased from Sinopharm Chemical Reagents Beijing Co. Water was supplied with a Barnstead Nanopure Water System (18.3 MΩ cm).

Synthesis of the Co nanoparticles@nitrogen-doped graphene film (Co@NGF)

Graphene oxide was first prepared by acid oxidation of graphite powders according to the modified Hummers method.[30] The flexible Co@NGF was fabricated by the vacuum filtration method combined with subsequently controlled calcination, which is displayed in Scheme 1. Typically, 80 mg of cobalt acetate and 30 mg of dicyandiamide were co-dissolved in 20 mL of water–ethanol solution (v/v = 1 : 1). The mixture was stirred at 80 °C for 1 h to form a dicyandiamide–Co complex, and then 10 mL of graphene oxide suspension (5 mg mL^{-1}) was added into the mixture and stirred for 1 h. Afterwards, the mixture was vacuum filtered through a membrane (200 nm pore size) to obtain a filter film, which was then vacuum dried for 24 h to obtain a dicyandiamide–Co@graphene film. Subsequently, the dicyandiamide–Co@graphene film was placed into a covered crucible in a tube furnace, which was annealed to 450 °C for 2 h, and then at 700 °C for another 2 h under Ar protection at a heating rate of 5 °C min^{-1}. The obtained black flexible Co nanoparticles@nitrogen-doped graphene film (Co@NGF) was then dipped in a 0.5 M HCl aqueous solution for 12 h to remove unwrapped Co nanoparticles. For comparison, hybrid films were also synthesized by the same procedure but without the addition of cobalt acetate or dicyandiamide or both, which were denoted as N-doped graphene film (NGF), Co nanoparticles embedded in graphene film (Co@GF) and graphene film (GF), respectively. Co@NGFs with different thicknesses were synthesized by the same procedure, while adding different amounts of mixture in the suction filter process.

Characterization

Field-emission scanning electron microscopy (FESEM, NOVA NANO SEM 430, FEI) measurements were employed to characterize the morphologies of the as-prepared samples. Transmission electron microscopy (TEM) measurements were carried out with a JOEL JEM 2100F microscope. Powder X-ray diffraction (XRD) patterns of the samples were recorded on a Bruker D8 Advance powder X-ray diffractometer with Cu Kα (λ = 0.15406 nm) radiation. X-ray photoelectron spectroscopy (XPS) measurements were performed using an ESCALAB 250. Raman spectra were acquired on a RENISHAW inVia instrument with an Ar laser source of 488 nm in a macroscopic configuration. The BET surface area was determined by using a Micromeritics ASAP 2010 with nitrogen adsorption at 77 K and the Barrett–Joyner–Halenda (BJH) method.

Electrochemical measurements

Electrochemical measurements were performed with an electrochemical workstation (CHI 760C, CH Instruments Inc.) in a 0.5 M H_2SO_4 aqueous solution. A Hg/Hg_2Cl_2 electrode (saturated KCl) and a platinum wire were used as the reference and counter electrode, respectively. The Co@NGF was cut into 1 × 0.5 cm^2. The film was used as the electrode directly and current densities were evaluated in terms of the film electrode area. Before testing, the Co@NGF was dipped in the 0.5 M H_2SO_4

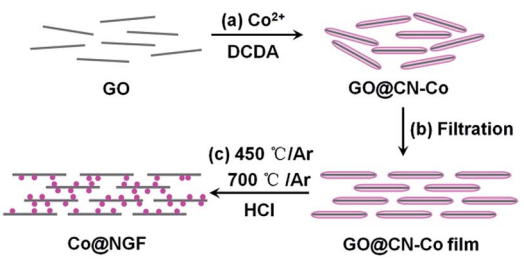

Scheme 1 Schematic illustration of the synthesis of Co@NGFs. (a) Adsorption of Co^{2+} and dicyandiamide (DCDA) onto graphene oxide nanosheets; (b) an efficient vacuum filtration; and (c) decomposition of dicyandiamide and reduction of Co^{2+} to form a Co@N-doped graphene film (Co@NGF).

electrolyte to enhance the wettability between the electrode and electrolyte. Polarization curves were acquired by sweeping the potential from 0 to −0.8 V (*vs.* Hg/Hg_2Cl_2) at a potential sweep rate of 5 mV s^{-1} in 0.5 M H_2SO_4. The accelerated stability tests were performed in 0.5 M H_2SO_4 at room temperature by potential cycling between 0 and −0.6 V (*vs.* Hg/Hg_2Cl_2) at a sweep rate of 100 mV s^{-1} for a given number of cycles. Current–time responses were monitored by chronoamperometric measurements for 50 000 s. The Nyquist plots were obtained with frequencies ranging from 100 kHz to 0.1 Hz at various overpotentials. Besides, we also studied the OER activity of Co@NGFs in 0.5 M H_2SO_4. Water electrolysis was carried out using Co@NGFs as both the anode and cathode in the two-electrode system in 0.5 M H_2SO_4. In all measurements, the Hg/Hg_2Cl_2 reference electrode (SCE, in saturated KCl) was calibrated with a reversible hydrogen electrode (RHE). E (RHE) = E (SCE) + 0.059 pH + 0.242 V.

Results and discussion

The morphology of the as-prepared Co@NGF was analysed by using a field emission scanning electron microscope (FESEM). Fig. 1a shows the highly flexible self-supported Co@NGF with a thickness of ~30 μm. A digital photo of the obtained Co@NGF (10 mm × 30 mm) is presented in the inset of Fig. 1a. From the cross-sectional view at high magnification, a layer by layer alternate structure is visible (Fig. 1b). Inside the film, there are hierarchical pores ranging from tens of nanometers to hundreds of nanometers intra- and inter-layers, resulting from the cross-linking of graphene sheets, unwrapped Co nanoparticles as templates (Fig. S1a†) and gas produced by the decomposition of dicyandiamide (Fig. S1b†). In addition, N_2 adsorption–desorption isotherms were measured to estimate the specific surface area and pore volume of the materials. As shown in Fig. S2,† the specific surface area of the Co@NGF is estimated to be 104.5 m^2 g^{-1}, and the pore size distribution curve (PSD, inset in Fig. S2†) is broad, ranging from tens of nanometers to over one hundred nanometers, which is evidenced by SEM. By contrast, the films produced from pure graphene nanosheets are solid without porous structure (Fig. S1c†). It can be seen that the surface of the Co@NGF is rippled and decorated with some objects that are most likely wrapped Co nanoparticles. It is noted that most of the unwrapped Co nanoparticles in the Co@NGF are removed by 0.5 M HCl (Fig. S3†). Energy dispersive X-ray spectroscopy (EDS) elemental mapping also shows a homogeneous distribution of C, N and Co elements throughout the Co@NGF (Fig. S4†).

The Co@NGF was further demonstrated by XRD and Raman spectra in Fig. 1c and d. The XRD patterns of the Co@NGF show an intense broad peak at 25.9° that is in good agreement with the (002) plane of graphitic carbon.[31,32] There is an additional weak peak at *ca.* 44.1°, which is consistent with the (111) crystal plane of metallic Co (JCPDS no. 15-0806, cubic, $a = b = c =$ 0.354 nm), signifying the successful production of Co–C hybrids. Cobalt nanoparticles were also confirmed by the analysis of the Raman spectrum which shows two characteristic peaks of Co at about 469.2 and 672.9 cm^{-1} (Fig. 1f).[33] Raman

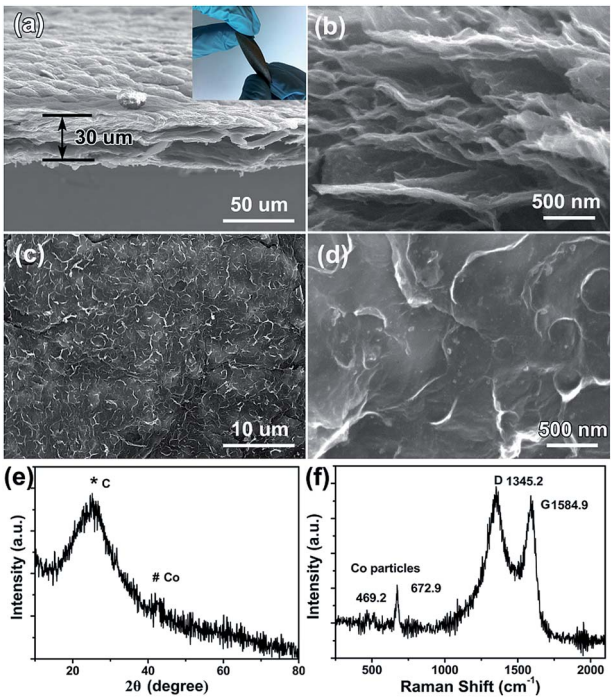

Fig. 1 Representative (a–d) SEM images, (e) XRD and (f) Raman results of Co@NGFs. The inset of (a) is the photo of the composite film. (b–d) are the cross-sectional view and surface structure at high magnification, respectively.

spectroscopic studies also show the D band (1345.2 cm^{-1}) and G band (1584.9 cm^{-1}) for graphene. The peak intensity I_D/I_G obtained from the Co@NGF is 1.05, indicating the increased sp^3 hybridization of carbon and the defects.[34]

Transmission electron microscopy (TEM) was then carried out to further determine the structure of the Co@NGF (Fig. 2). Fig. 2a and b show that the graphene nanosheets (grey background) are decorated with some dark-contrast Co nanoparticles with a particle size distribution of about 20–90 nm (Fig. S5†). From Fig. 2c, the Co (111) crystal planes can be clearly seen with a lattice spacing of 2.04 Å. The TEM results also imply that the Co nanoparticles are protected by graphene, which cannot be removed by acid washing.

The composition and valence states of Co@NGFs were determined by XPS measurements. As depicted in Fig. 3a, the elements of carbon, nitrogen, oxygen and cobalt can be easily identified. As shown in Fig. 3b, a major peak appeared at 284.5 eV belongs to the C element, which is the characteristic peak of C1s. The N1s spectrum of the Co@NGF shows the

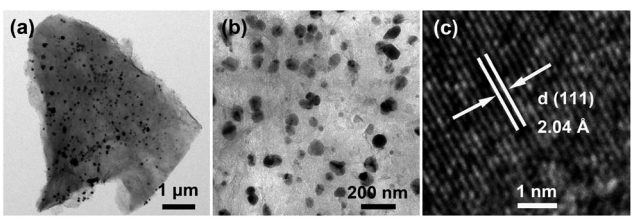

Fig. 2 (a and b) TEM images of the Co@NGF at different magnifications, (c) HRTEM image of Co nanoparticles in the Co@NGF.

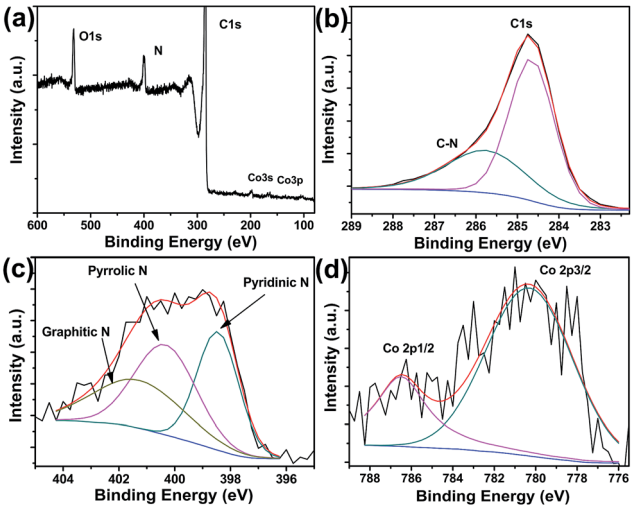

Fig. 3 (a) XPS survey spectra and high-resolution scans of (b) C1s, (c) N1s and (d) Co2p electrons of Co@NGFs.

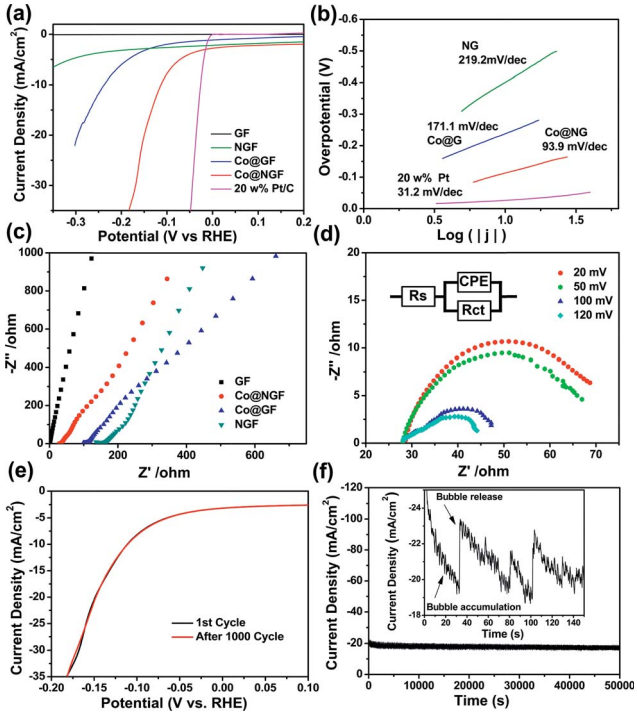

Fig. 4 (a) Polarization curves (iR corrected) for the HER in 0.5 M H_2SO_4 of 20 wt% Pt/C, Co@NGF, Co@GF, NGF and GF, respectively. Potential sweep rate 5 mV s^{-1}. (b) Corresponding Tafel plots (overpotential *versus* log current density) derived from (a). (c) Nyquist plots of the Co@NGF, Co@GF, NGF and GF at open circuit potential. (d) Nyquist plots and the equivalent circuit of the Co@NGF at various HER overpotentials in 0.5 M H_2SO_4. (e) HER polarization curves of the Co@NGF before and after 1000 cycles in the stability test. (f) Current–time plots of the Co@NGF at the applied potential of −0.20 V (*vs.* RHE). The inset shows the impact of bubbles formed on the electrode surface on the HER currents.

presence of graphitic *N* (401.3), pyrrolic *N* (400.3 eV) and pyridinic *N* (398.4 eV) in Fig. 3c, indicating the successful incorporation of N into the graphene matrix.[35] N doping was also observed in the survey spectrum of C1s electrons in Fig. 3b, which shows a characteristic peak of C–N (285.8 eV).[36] Deconvolution of the high-resolution scan of the Co2p electrons yields a pair of peaks at 786.5 and 780.3 eV (Fig. 3d), respectively.[36,37] Furthermore, based on the integrated peak areas, the atomic contents of Co and N in the Co@NGF are estimated to be 0.8 and 4.9 at%, respectively.

The Co@NGF was directly investigated as the electrode for the HER in 0.5 M H_2SO_4 at a scan rate of 5 mV s^{-1}. The Co@GF, NGF, GF and 20 wt% Pt/C loaded on Ti mesh (at a loading of 0.28 mg cm^{-2}) were also tested for comparison in Fig. 4a. A polarization curve recorded by the as-prepared Co@NGF shows a low overpotential (η) of −14 mV for the HER that is very close to the commercial 20 wt% Pt/C loaded on Ti mesh (−2 mV), with a sharp increase in cathodic current, corresponding to catalytic H_2 evolution. In addition, the Co@NGF shows a low overpotential of −124.6 mV at a current density (j) of 10 mA cm^{-2}. By contrast, the Co@GF and NGF reveal inferior HER activity with larger onset potentials of −105.1 and −196.5 mV, respectively. Furthermore, the GF shows no HER activity as no reduction current even at the −520 mV. The aforementioned results indicate the significant synergistic effect between N-doped graphene and Co nanoparticles on the determination of the Co@NGF HER activity.

The Tafel plots derived from Fig. 4a are shown in Fig. 4b, where their linear portions were fitted to the Tafel equation to determine Tafel slopes. Note that for hydrogen evolution in acid media on electrode surfaces, the mechanism typically involves three major reactions,[7,12,38]

$$H_3O^+ + \text{e-catalyst} \leftrightarrow \text{H-catalyst} + H_2O \text{ (Volmer reaction, 120 mV per dec)} \quad (1)$$

$$2\text{H-catalyst} \leftrightarrow H_2\text{-catalyst (Tafel reaction, 30 mV per dec)} \quad (2)$$

$$H_3O^+ + \text{e-catalyst} + \text{H-catalyst} \leftrightarrow H_2\text{-catalyst} + \text{catalyst} + H_2O \text{ (Heyrovsky reaction, 40 mV per dec)} \quad (3)$$

where e-catalyst denotes metal-bound electrons, and H-catalyst and H_2-catalyst represent a hydrogen atom and a hydrogen molecule adsorbed onto a surface atom of the catalyst, respectively.

The Tafel slope is estimated to be 93.9 mV per dec for the Co@NGF, which suggests that the rate-determining step of the HER is most likely the Volmer reaction, a discharge step that converts protons into adsorbed hydrogen atoms on the catalyst surface. Note that much higher Tafel slopes (171.1 and 219.2 mV per dec) are observed for the Co@GF and NGF, respectively, which are consistent with their lower HER activity.

The robust and flexible Co@NGF as the HER electrode with an onset potential of −14 mV, a Tafel slope of 93.9 mV per dec and a high current density of 10 mA cm^{-2} at −124.6 mV compares favorably with those of HER film electrodes in the acidic aqueous electrolyte, such as porous C_3N_4 nanolayers@N-graphene films,[26] edge-oriented MoS_2 nanoporous films,[39] cobalt sulfide nanosheet/graphene/carbon nanotube nanocomposites,[20] Molybdenum sulfide cluster-nitrogen-doped graphene hybrid hydrogel films,[28] MoS_2 nanoflower-decorated reduced graphene oxide paper,[40] and reduced graphene oxide-modified carbon nanotube/polyimide films,[41] which are summarized in Table S1.†

The HER kinetics at the electrode/electrolyte interface was further investigated by electrochemical impedance spectroscopy (EIS, tested at various potentials, Fig. 4c and d). The series resistance (R_s) data were obtained in the high frequency zone and then were used to correct the polarization curves. The R_s value of the Co@NGF is about 27.5 Ω, which is lower than that of the Co@GF (98.8 Ω) and NGF (136.3 Ω), but higher than that of the GF (1.0 Ω). In addition, the charge transfer resistance (R_{ct}) is related to the electrocatalytic kinetics and its lower value corresponds to the faster reaction rate, which can be obtained from the semicircle in the low frequency zone.[42] The R_{ct} of the Co@NGF was found to decrease significantly with increasing overpotentials, from ~55 Ω at −20 mV to ~17.5 Ω at −120 mV, suggesting the fast electron transfer and the favorable HER kinetics at the electrolyte interface.

Durability is another important criterion to evaluate the performance of HER electrodes. The cycle performance was investigated using polarization curves. Fig. 4e shows that, even after 1000 potential cycles, the *j*–*V* curve of the Co@NGF electrode remains almost unchanged, indicating the long-term viability under operating conditions. To further verify the stability of the Co@NGF for the HER, the current–time plots at an applied potential of −0.20 V (*vs.* RHE) was depicted in Fig. 4f. The catalytic current remains unchanged for 50 000 s of continuous operation, indicating strong durability of the Co@NGF electrode for the HER in 0.5 M H_2SO_4.

The Co@NGFs with different thicknesses of 1.2, 14.5, 30 and 40 μm have a similar porous film microstructure (Fig. 5a). The hierarchical pores are generated intra- and inter-layers in the films due to the interlocking-tile cross-linking and the corrugated configuration of graphene sheets. The corresponding polarization curves of Co@NGFs with different thicknesses are shown in Fig. 5e. The catalytic current densities increased from 11.8 mA cm^{-2} at −200 mV for the 1.2 μm film to 25.3 mA cm^{-2} at −200 mV for the 30 μm film, indicating the catalytic activity of the Co@NGF derived from N-doped graphene shells with promotion of Co nanoparticles as the core. These results are also confirmed by other reported results,[23] in which, the

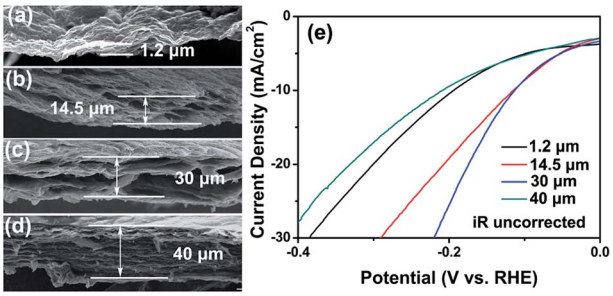

Fig. 5 (a–d) SEM images and (e) polarization curves of Co@NGF with different thicknesses.

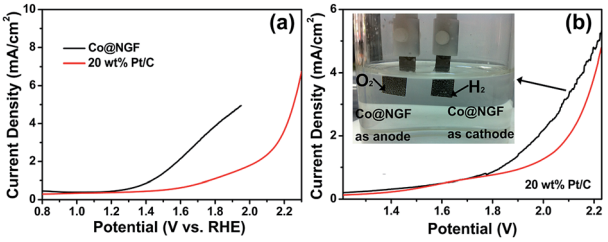

Fig. 6 (a) Polarization curves for the oxygen evolution reaction (OER) in 0.5 M H_2SO_4 of the Co@NGF and 20 wt% Pt/C in the three-electrode system. (b) Polarization curves of Co@NGFs and 20 wt% Pt/Cs as both the HER electrode and OER electrode in 0.5 M H_2SO_4 in the two-electrode system. Inset is the optical photograph showing the generation of H_2 and O_2 bubbles on Co@NGF electrodes.

ultrathin graphene shells strongly promote electron penetration from the CoNi nanoalloy to the graphene surface. However, the catalytic activity of the Co@NGF with a thickness of 40 μm possesses the decreased current density of 10.2 mA cm^{-2} at −200 mV, implying the non-linear relationship between thicknesses and HER activity, which are possibly due to the different pore structures of the Co@NGF. As shown in Fig. 5d, the Co@NGF with a thickness of 40 μm possesses a smaller amount of porous structure possibly due to a bigger gathering force during the suction filter process.

A lot of studies have focused on the research of HER electrocatalysts with low overpotentials and high current densities in acidic media, such as MoS_2,[10,43–46] MoC_2,[47,48] MoP,[49] Ni_2P,[50] CoSe,[51] Co@carbon,[18,21–23] and N, S-doped carbon,[52,53] because the high concentration of protons is more facile for the hydrogen evolution. On the contrary, oxygen evolution is easier when the concentration of hydroxide is high. To realize the overall water splitting, highly active OER catalysts need to be developed in acidic media. Herein, the Co@NGF was also confirmed to be electrochemically active toward the OER in 0.5 M H_2SO_4 (Fig. 6a). The onset potential of the Co@NGF is about 1.42 V *vs.* RHE, which is much better than that of 20 wt% Pt/C (about 1.81 V). Accordingly, we prepared a two-electrode system with 0.5 M H_2SO_4 solution as a medium by applying Co@NGFs as both the water reduction electrode and water oxidation electrode. The voltage of water-splitting reaction is about 1.83 V in the two-electrode system, which is also better than that of 20

wt% Pt/C (1.97 V). The obvious hydrogen and oxygen bubbles are observed on Co@NGF electrodes (inset to Fig. 6b). In addition, the cell exhibits considerable stability in nearly 24 000 s of continuous operation with a retention rate of 78.9% (Fig. S6†). Notably, there are a few reports about splitting water into H_2 and O_2 using the same nonprecious electrode as the anode and the cathode in acid media, which paves a new pathway for designing overall water splitting catalysts. However, the current density of water electrolysis using Co@NGFs in 0.5 M H_2SO_4 in the two-electrode system is low in our experiment, which needs to be further resolved.

Conclusions

In summary, this work reports a facile and easily scalable fabrication of cobalt nanoparticles wrapped by a N-doped graphene film (Co@NGF) based on earth-abundant and cost-effective components for the hydrogen evolution reaction. Co nanoparticles wrapped by N-doped graphene nanosheets were produced by decomposition of dicyandiamide and reduction of Co^{2+}. Electrochemical studies showed that the obtained film electrodes exhibited excellent HER activity with an onset potential of −14 mV (*vs.* RHE), a large current density, a small Tafel slope of 93.9 mV per dec, as well as prominent electrochemical durability. The excellent HER catalytic ability of the Co@NGF could be attributed to the synergetic effect among the core–shell structure, N-doped treatment and cobalt nanoparticles. Co@NGFs can be applied as water electrolysis electrodes for both the HER and OER in 0.5 M H_2SO_4 in two-electrode systems, which encourages us to explore overall water splitting catalysts in acid media.

Acknowledgements

This work was supported by the PhD Start-up Funds of the Natural Science Foundation of Guangdong Province (S2013040016465), and Zhujiang New Stars of Science & Technology (2014J2200061); the National Science Fund for Excellent Young Scholars of China (No. 51422203), National Natural Science Foundation of China (No. 51372001 and 51002052), Excellent Youth Foundation of Guangdong Scientific Committee (No. S2013050013882), and Key Project in Science and Technology of Guangdong Province (No. 2011A080801018).

Notes and references

1 M. G. Walter, E. L. Warren, J. R. McKone, S. W. Boettcher, Q. Mi, E. A. Santori and N. S. Lewis, *Chem. Rev.*, 2010, **110**, 6446–6473.
2 N. S. Lewis and D. G. Nocera, *Proc. Natl. Acad. Sci. U. S. A.*, 2006, **103**, 15729–15735.
3 W. Zhou, Z. Yin, Y. Du, X. Huang, Z. Zeng, Z. Fan, H. Liu, J. Wang and H. Zhang, *Small*, 2013, **9**, 140–147.
4 D. Gopalakrishnan, D. Damien and M. M. Shaijumon, *ACS Nano*, 2014, **8**, 5297–5303.
5 D. Kong, H. Wang, J. J. Cha, M. Pasta, K. J. Koski, J. Yao and Y. Cui, *Nano Lett.*, 2013, **13**, 1341–1347.
6 A. B. Laursen, S. Kegnæs, S. Dahl and I. Chorkendorff, *Energy Environ. Sci.*, 2012, **5**, 5577–5591.
7 Y. Li, H. Wang, L. Xie, Y. Liang, G. Hong and H. Dai, *J. Am. Chem. Soc.*, 2011, **133**, 7296–7299.
8 M. A. Lukowski, A. S. Daniel, F. Meng, A. Forticaux, L. Li and S. Jin, *J. Am. Chem. Soc.*, 2013, **135**, 10274–10277.
9 D. Voiry, H. Yamaguchi, J. Li, R. Silva, D. C. Alves, T. Fujita, M. Chen, T. Asefa, V. B. Shenoy and G. Eda, *Nat. Mater.*, 2013, **12**, 850–855.
10 J. Xie, H. Zhang, S. Li, R. Wang, X. Sun, M. Zhou, J. Zhou, X. W. D. Lou and Y. Xie, *Adv. Mater.*, 2013, **25**, 5807–5813.
11 J. Yang, D. Voiry, S. J. Ahn, D. Kang, A. Y. Kim, M. Chhowalla and H. S. Shin, *Angew. Chem., Int. Ed.*, 2013, **52**, 13751–13754.
12 W. Zhou, D. Hou, Y. Sang, S. Yao, J. Zhou, G. Li, L. Li, H. Liu and S. Chen, *J. Mater. Chem. A*, 2014, **2**, 11358–11364.
13 J. F. Callejas, C. G. Read, E. J. Popczun, J. M. McEnaney and R. E. Schaak, *Chem. Mater.*, 2015, **137**, 3769–3774.
14 P. Jiang, Q. Liu, C. Ge, W. Cui, Z. Pu, A. M. Asiri and X. Sun, *J. Mater. Chem. A*, 2014, **2**, 14634–14640.
15 Q. Liu, J. Tian, W. Cui, P. Jiang, N. Cheng, A. M. Asiri and X. Sun, *Angew. Chem.*, 2014, **126**, 6828–6832.
16 E. J. Popczun, C. G. Read, C. W. Roske, N. S. Lewis and R. E. Schaak, *Angew. Chem.*, 2014, **126**, 5531–5534.
17 Z. Xing, Q. Liu, W. Xing, A. M. Asiri and X. Sun, *ChemSusChem*, 2015, **8**, 1850–1855.
18 X. Zou, X. Huang, A. Goswami, R. Silva, B. R. Sathe, E. Mikmeková and T. Asefa, *Angew. Chem.*, 2014, **126**, 4461–4465.
19 N. Jiang, B. You, M. Sheng and Y. Sun, *Angew. Chem., Int. Ed.*, 2015, **54**, 6251–6254.
20 S. Peng, L. Li, X. Han, W. Sun, M. Srinivasan, S. G. Mhaisalkar, F. Cheng, Q. Yan, J. Chen and S. Ramakrishna, *Angew. Chem., Int. Ed.*, 2014, **53**, 12594–12599.
21 W. Zhou, Y. Zhou, L. Yang, J. Huang, Y. Ke, K. Zhou, L. Li and S. Chen, *J. Mater. Chem. A*, 2015, **3**, 1915–1919.
22 W. Zhou, J. Zhou, Y. Zhou, J. Lu, K. Zhou, L. Yang, Z. Tang, L. Li and S. Chen, *Chem. Mater.*, 2015, **27**, 2026–2032.
23 J. Deng, P. Ren, D. Deng and X. Bao, *Angew. Chem., Int. Ed.*, 2015, **54**, 2100–2104.
24 K. Gong, F. Du, Z. Xia, M. Durstock and L. Dai, *Science*, 2009, **323**, 760–764.
25 W. Zhou, K. Zhou, D. Hou, X. Liu, G. Li, Y. Sang, H. Liu, L. Li and S. Chen, *ACS Appl. Mater. Interfaces*, 2014, **6**, 21534–21540.
26 J. Duan, S. Chen, M. Jaroniec and S. Z. Qiao, *ACS Nano*, 2015, **9**, 931–940.
27 J. Ren, M. Antonietti and T. P. Fellinger, *Adv. Energy Mater.*, 2015, **5**, DOI: 10.1002/aenm.201570029.
28 S. Chen, J. Duan, Y. Tang, B. Jin and S. Z. Qiao, *Nano Energy*, 2015, **11**, 11–18.
29 Y. H. Chang, C. T. Lin, T. Y. Chen, C. L. Hsu, Y. H. Lee, W. Zhang, K. H. Wei and L. J. Li, *Adv. Mater.*, 2013, **25**, 756–760.
30 W. S. Hummers Jr and R. E. Offeman, *J. Am. Chem. Soc.*, 1958, **80**, 1339.

31 R. Elazari, G. Salitra, A. Garsuch, A. Panchenko and D. Aurbach, *Adv. Mater.*, 2011, **23**, 5641–5644.
32 Z.-Z. Jiang, Z.-B. Wang, Y.-Y. Chu, D.-M. Gu and G.-P. Yin, *Energy Environ. Sci.*, 2011, **4**, 2558–2566.
33 R. B. Rakhi, W. Chen, D. Cha and H. N. Alshareef, *Nano Lett.*, 2012, **12**, 2559–2567.
34 Y. Huh, J. Y. Lee, J. Cheon, Y. K. Hong, J. Y. Koo, T. J. Lee and C. J. Lee, *J. Mater. Chem.*, 2003, **13**, 2297–2300.
35 L. Qu, Y. Liu, J.-B. Baek and L. Dai, *ACS Nano*, 2010, **4**, 1321–1326.
36 N. Wu, L. Fu, M. Su, M. Aslam, K. C. Wong and V. P. Dravid, *Nano Lett.*, 2004, **4**, 383–386.
37 M. C. Biesinger, B. P. Payne, A. P. Grosvenor, L. W. Lau, A. R. Gerson and R. S. C. Smart, *Appl. Surf. Sci.*, 2011, **257**, 2717–2730.
38 Y. Zheng, Y. Jiao, M. Jaroniec and S. Z. Qiao, *Angew. Chem., Int. Ed.*, 2015, **54**, 52–65.
39 Y. Yang, H. Fei, G. Ruan, C. Xiang and J. M. Tour, *Adv. Mater.*, 2014, **26**, 8163–8168.
40 C.-B. Ma, X. Qi, B. Chen, S. Bao, Z. Yin, X.-J. Wu, Z. Luo, J. Wei, H.-L. Zhang and H. Zhang, *Nanoscale*, 2014, **6**, 5624–5629.
41 Y. Jiang, X. Li, S. Yu, L. Jia, X. Zhao and C. Wang, *Adv. Funct. Mater.*, 2015, **25**, 2693–2700.
42 L. Liao, J. Zhu, X. Bian, L. Zhu, M. D. Scanlon, H. H. Girault and B. Liu, *Adv. Funct. Mater.*, 2013, **23**, 5326–5333.
43 L. Yang, W. Zhou, D. Hou, K. Zhou, G. Li, Z. Tang, L. Li and S. Chen, *Nanoscale*, 2015, **7**, 5203–5208.
44 Y. Sun, S. Gao, F. Lei and Y. Xie, *Chem. Soc. Rev.*, 2015, **44**, 623–636.
45 M.-R. Gao, J.-X. Liang, Y.-R. Zheng, Y.-F. Xu, J. Jiang, Q. Gao, J. Li and S.-H. Yu, *Nat. Commun.*, 2015, **6**, 5982.
46 N. Liu, L. Yang, S. Wang, Z. Zhong, S. He, X. Yang, Q. Gao and Y. Tang, *J. Power Sources*, 2015, **275**, 588–594.
47 L. Liao, S. Wang, J. Xiao, X. Bian, Y. Zhang, M. D. Scanlon, X. Hu, Y. Tang, B. Liu and H. H. Girault, *Energy Environ. Sci.*, 2014, **7**, 387–392.
48 H. B. Wu, B. Y. Xia, L. Yu, X.-Y. Yu and X. W. D. Lou, *Nat. Commun.*, 2015, **6**, 6512.
49 Z. Xing, Q. Liu, A. M. Asiri and X. Sun, *Adv. Mater.*, 2014, **26**, 5702–5707.
50 E. J. Popczun, J. R. McKone, C. G. Read, A. J. Biacchi, A. M. Wiltrout, N. S. Lewis and R. E. Schaak, *J. Am. Chem. Soc.*, 2013, **135**, 9267–9270.
51 D. Kong, H. Wang, Z. Lu and Y. Cui, *J. Am. Chem. Soc.*, 2014, **136**, 4897–4900.
52 X. Liu, W. Zhou, L. Yang, L. Li, Z. Zhang, Y. Ke and S. Chen, *J. Mater. Chem. A*, 2015, **3**, 8840–8846.
53 Y. Ito, W. Cong, T. Fujita, Z. Tang and M. Chen, *Angew. Chem., Int. Ed.*, 2014, **54**, 2131–2136.